ELSEVIER

CrossMark

Journal of the European Ceramic Society 34 (2014) 753–763

www.elsevier.com/locate/jeurceramsoc

Quantitative analysis of the residual stress and dislocation density distributions around indentations in alumina and zirconia toughened alumina (ZTA) ceramics

S. Huang [a,*], J.G.P. Binner [a], B. Vaidhyanathan [a], R.I. Todd [b]

[a] *Department of Materials, Loughborough University, Loughborough, Leicestershire LE11 3TU, UK*
[b] *Department of Materials, University of Oxford, Oxford OX1 3PH, UK*

Received 13 June 2013; received in revised form 16 September 2013; accepted 28 September 2013
Available online 2 November 2013

Abstract

Alumina, 10% and 20% ZTA with 1.5 mol% yttria stabiliser were subjected to Vickers indentation testing with loads from 1 to 20 kg. Cr^{3+} fluorescence and Raman spectroscopy were applied to the indent centre and around the indentation in order to investigate the origin of the signal, the effect of indentation loads and zirconia phase transformation on the residual stress and plastic deformation in the plastic zone. The results suggested that with very strong laser scattering, the depth resolution of ZTA materials was very poor, which lead to a very significant amount of the signal being collected from the subsurface regions below the plastic zone. It was also found that zirconia phase transformation reduced the compressive residual stress in the alumina matrix within the plastic zone, except at the indentation centre, due to the tensile residual microstress generated by the zirconia phase transformation. In addition, the dislocation density on the indent surface of the ZTA samples was significantly reduced due to the restriction of crack propagation and energy absorption during the phase transformation process. At the indent centre, the zirconia phase transformation was suppressed by the high compressive stress, therefore, no significant difference between alumina and ZTA in terms of their residual stress and dislocation density were observed. Using TEM observation, it was found that the plastic zone microstructure of pure alumina is different from that of ZTA, which is consistent with the Cr^{3+} fluorescence results.

Keywords: Zirconia phase transformation; Residual stress; Dislocation density; 4-Peak fitting; Indentation

1. Introduction

Zirconia toughened alumina (ZTA) has been extensively researched due to its outstanding properties of high toughness, hardness, wear resistance and chemical stability.[1–3] The zirconia additions toughen the alumina matrix via the tetragonal to monoclinic transformation that occurs in the stress field of growing cracks. The phase transformation results in a 4–5 vol% expansion, which provides a compressive stress that acts to reduce the propagation of the crack. Zirconia toughened alumina (ZTA) is already being used in a wide range of applications, from cutting tools, wear parts and biomechanical devices to ballistic protection.[4,5]

Whilst the Vickers indentation toughness measurement technique is not a rigorous approach, it can be used to obtain a rough indication of the resistance to crack propagation in ceramics. Katagiri[6] has measured the amount of zirconia phase transformation around indents on pure zirconia using Raman spectroscopy and then quantitatively calculated the zirconia phase transformability. In addition, a Vickers indent leaves a plastically deformed zone beneath it. Generating, a better understanding of the residual stress and plastic deformation conditions induced by indentation in ZTA ceramics can help to investigate the effect of zirconia phase transformation on the plastic deformation of the alumina matrix and the stress field distribution after the indentation test.

For alumina-based ceramics, the residual stress can be investigated using Cr^{3+} fluorescence spectroscopy.[7–10] Using an optical microprobe, a laser is focused on the sample surface. The chromium ions, Cr^{3+}, a persistent impurity in alumina, interact with the laser and result in luminescence. When the crystal of

* Corresponding author. Tel.: +44 01509 223330; fax: +44 01509 223949.
E-mail addresses: s.huang2@lboro.ac.uk, s.huang12@outlook.com (S. Huang).

0955-2219/$ – see front matter © 2013 Elsevier Ltd. All rights reserved.
http://dx.doi.org/10.1016/j.jeurceramsoc.2013.09.021

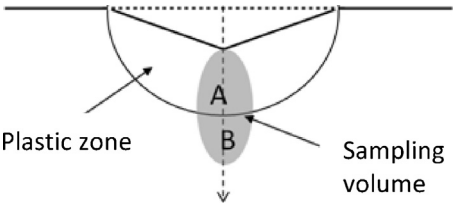

Fig. 1. Schematic of the sampling volume at the centre of the indent in alumina, where regions both inside the plastic zone (A) and outside it (B) are sampled simultaneously.[13]

the material is subject to a stress, the frequency of the luminescent peaks in the spectrum shifts correspondingly, allowing an indication of the mean stress distribution to be obtained.[7,11] In a polycrystal with randomly orientated grains the relationship between the mean peak shift and the hydrostatic component of the residual stress in the crystal is given by:

$$\Delta v = \Pi_H \sigma_H \quad (1)$$

where $\Delta\nu$ is the peak shift (cm^{-1}) relative to the stress-free peak position, σ_H is the hydrostatic stress component (GPa) and Π_H is the appropriate piezo-spectroscopic coefficient, which has a value of 7.6 cm^{-1} for the R1 peak.[8]

Guo and Todd[12,13] have observed that the axial resolution of the microscope and the translucency of the material can significantly affect Cr^{3+} fluorescence analysis. Studying the centre of an indent made in alumina using a 1 kg load revealed a single curve that contained four overlapping peaks, two broad peaks and two sharp peaks. By characterising the probe response function (PRF) and fitting the four peaks with an appropriate physical constraint, the two broad peaks were confirmed to originate from the plastic zone of the indentation, whilst the two sharp peaks were believed to have arisen from the elastically deformed region beneath it (Fig. 1). The relatively high transparency of alumina meant that the laser could penetrate below the surface on which it was focused, leading to a large sampling volume covering both the material in the plastic zone and the subsurface region. This indicates that the axial resolution of the Cr^{3+} fluorescence spectroscopy is not only controlled by the resolution of the equipment, but also by the transparency of the material. In order to investigate the residual stress distribution caused by the indentation of the ZTA ceramics, it is essential to determine the resolution of the microscope and the laser penetration depth so that it is possible to determine which fluorescence peaks represent the signal from the plastic zone.

In addition to the peak shift analysis, Ma et al.[8] also established that the fluorescence peaks from a plastically deformed material region, such as a plastic zone formed by an indentation, broaden significantly due to the resulting stress variations within the sampling volume. This was important as it demonstrated that the level of plastic deformation arising from dislocations having a high local stress field could be quantitatively determined from within a probed volume. According to an experimental and modelling study by Wu et al.,[11] the R1 peak broadening, $\sqrt{\langle \Delta\nu^2 \rangle}$, is proportional to the dislocation density, ρ, in the probed position:

$$\sqrt{\langle \Delta\nu^2 \rangle} = kF(\rho) \quad (2)$$

where k is a constant related to the lattice parameters of the alumina crystal and the piezo-spectroscopic coefficients and $F(\rho)$ is a function correlated with the dislocation density.

In this work, three materials have been prepared and characterised, viz. monolithic alumina, 10% ZTA and 20% ZTA, where the zirconia additions were partially stabilised using 1.5 mol% yttria. The grain size of the alumina phase was the same in each case. A high-resolution, confocal micro-Raman spectroscope was used to study the spatial distribution of indentation-induced phase transformations in the ZTA materials and Cr^{3+} fluorescence analysis was used to determine the residual stresses around the indents. All the samples were subject to four indentation loads, viz. 1, 5, 10 and 20 kg, in order to validate the four peak fitting approach introduced by Guo and Todd and quantitatively analyse the residual stress under different indentation loads.

2. Experimental

2.1. Sample preparation

As received, aqueous YSZ nanosuspension containing 1.5 mol% yttria (MEL Chemicals, Manchester, UK) was mixed with a fine submicron alumina aqueous suspension (Baikowski, Annecy, France), to form suspensions containing 0, 10 and 20 wt% YSZ in the final materials. Details of the as-received suspensions are listed in Table 1. In order to achieve a high density green body, the as-mixed suspensions, which had solid contents of 40–50 wt%, were further concentrated to ~57 wt%. During the concentration, the suspensions were subjected to ultrasonic treatments every 30 min using an ultrasonicator (MSE Scientific Instruments, Manchester, UK) to break up any agglomerate that formed and hence to control the viscosity of the suspensions at ~80 mPa at 100 s^{-1} shear rate. Full details of the concentration method have been provided elsewhere.[14,15]

The suspensions were then spray freeze dried to yield granules that possessed high flowability, due to their spherical shape, and high crushability, due to their porous structure after the ice was sublimed. A foaming agent consisting of 2 vol% Freon (trichlorofluoromethane, Fisher Scientific UK Limited, UK) was added to the high solid content suspensions prior to the spray freeze drying to improve the granule crushability. In the spray freezing stage, the suspension was dripped onto an ultrasonic rod using a pipette so that droplets were formed that subsequently fell into liquid nitrogen and froze. The beakers containing the frozen granules were subsequently connected to a freeze dryer (Virtis®, Benchtop SLC, New York, USA), that was connected in turn to a double stage, oil-sealed, rotary vane vacuum pump (Leybold® D2.5B, Leybold vacuum GmbH, Oberkochen, Germany) with an exhaust filter allowing the droplets to be freeze dried under a vacuum of <100 mTorr at −50 °C; the process took about 2 days. Full details of the spray freeze drying method have been provided elsewhere.[16]

After drying, the granulated powder was sieved to achieve granules in the range 125–250 μm and die pressed at 250 MPa to achieve green densities of ~55% of theoretical. The pellets, which measured 10 mm diameter and 4 mm thickness, were then sintered at temperatures in the range 1400–1500 °C with

Table 1
The properties of the as-received nanosuspensions.

Name	Yttria content (mol%)	Solid content (wt%)	pH	Particle size (D50) (nm)
1.5YSZ	1.5	26.5	2.50	13
Alumina	–	58.8	3.52	160

Table 2
Processing and microstructural properties of samples.

Sample code	Sintering T (°C)	Hold time (h)	Density (% theor.)	Mean grain size	
				Al_2O_3 (μm)	YSZ (nm)
Alumina	1400	10	99.0 ± 0.2	1.2	–
10% ZTA	1450	10	99.0 ± 0.2	0.9 ± 0.1	170 ± 60
20% ZTA	1500	10	99.3 ± 0.3	1.1 ± 0.1	280 ± 60

a constant heating rate of 10 °C min^{-1} and hold time of 10 h in order to achieve densities of >99%. The alumina grain sizes were ~1 μm in all samples, thus eliminating grain size variations from having an effect on the mechanical properties. The crystalline phases of the zirconia grains in the ZTA materials were analysed using X-ray diffraction (XRD), the result indicated that both the 10% and 15% ZTA showed 100% tetragonal zirconia phase. The details of the sintering conditions and the resultant densities and grain sizes are listed in Table 2.

2.2. Indentation

All specimens were sequentially polished using a series of diamond grits of 9, 3 and 1 μm grit size. Each step of the polishing sequence was performed for sufficient time to eliminate all surface damage induced by the previous step. 1 kg Vickers hardness indentations were made on the polished surfaces with 15 s loading time using a HM-124 micro indentation hardness tester (Mitutoyo, Japan) and an AVK-C2 hardness tester (Mitutoyo, Japan) was used to indent the samples using 5, 10 and 20 kg loads. For all three ceramics and for each load/sample combination at least 5 indents were made. The indentation hardness and toughness values of the samples were collected using the 1 and 10 kg indentation, respectively.

To allow the plastic zone for each indent to be examined, two polished samples were bonded together using superglue and then the top, joined surface was polished again to 1 μm grit size. The indentations were then made along the join line and the two samples separated by dissolving the glue in acetone. A schematic drawing is shown in Fig. 2(a). The plastic zone was observed using optical microscopy, as shown in Fig. 2(b), and its size confirmed to be similar to the half-length of the diagonal of the indent.

2.3. Determination of the zirconia phases

The zirconia phases present in and around the indents were investigated using a high-resolution confocal Raman spectrometer (Horiba Yvon Raman LabramHR, Horiba Jobin Yvon SAS, Villeneuve d'Ascq, France) equipped with a liquid nitrogen cooled CCD detector and incident radiation from a He red laser at 633 nm. The laser power was 20 mW, the spectrum integration

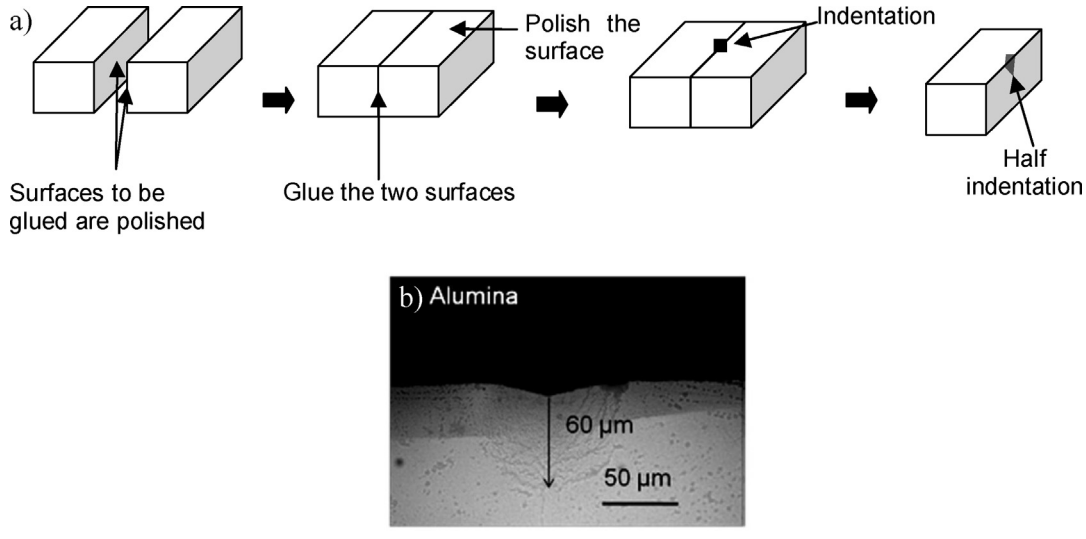

Fig. 2. (a) Schematic of the sample preparation for plastic zone observation and (b) optical microscopy image showing the plastic zone of an alumina sample.

time was 40 s and an objective lens with 100× magnification was used. Raman spectra between 100 and 400 cm^{-1} were recorded. This range was selected as the main monoclinic bands are at 181 and 192 cm^{-1}, whilst the primary tetragonal bands are at 148 and 264 cm^{-1}.[6,17]

A line scan of the zirconia phase transformation from the sample surface outside the indent towards its centre was carried out. The laser was first focused on the polished surface and then scanned towards the indent centre, the scanning lines were 60 μm long with a step of 3 μm and the laser was auto-focused at each step. The transformed monoclinic zirconia concentration (m) was quantitatively determined using the equation[17]:

$$m = \frac{1/2(I_m^{181} + I_m^{192})}{0.97(I_t^{148} + I_t^{264}) + 1/2(I_m^{181} + I_m^{192})} \quad (3)$$

where I is the intensity of the peaks and the subscript indicates the corresponding phase, whilst the superscript indicates the peak position in reciprocal centimetres.

2.4. Cr^{3+} fluorescence spectroscopy

Cr^{3+} fluorescence spectra were obtained using the same equipment as was used for the Raman spectra in section 2.3. The smallest surface spot size of 1.5 μm was achieved using a 100× objective lens and a confocal aperture of 20 μm diameter (the spot size was measured by focusing the laser on a SiC surface and then measuring the size of the light spot directly). For each measurement, a region of interest was selected using the optical microscope with white light.

The Cr^{3+} fluorescence analysis was carried out in two stages. Firstly, a depth scan[12] was performed to investigate the confocal resolution and degree of laser transparency of each sample. To achieve this, the laser was initially focused on each 1 μm polished sample surface at a remote location from the indents, this position was set as zero; then the specimen stage was moved upward by 100 μm, so that the laser focal plane was below the surface. Scanning was then carried out in the direction normal to the sample surface in 2 μm steps from the starting position, −100 μm, to +50 μm above the surface with the Cr^{3+} fluorescence spectra being collected at each step. Secondly, line scanning was again performed as described in Section 2.3, but this time collecting the Cr^{3+} fluorescence spectra. Note that for both the depth scanning and line mapping, the results were repeatable.

The collected data were subsequently analysed with a constrained 4-peak fitting method[13,18] using fitting software, Auto2Fit 5.5 (7-D software, China). Essentially, two doublets of the R1 and R2 peaks were fitted using a mixed Lorentzian and Gaussian function subject to the constraint that the R1 to R2 peak area ratio for any individual doublet was equal to 2.0.[13] Finally, the peak position and width were identified and used to investigate the residual stresses and dislocation densities after each indentation test. Since a certain amount of residual stresses could be generated during the sintering process and, particularly, surface polishing, all the peak shifts and broadenings of the indentation-tested samples were compared with data obtained after sintering and polishing but before indenting.

2.5. FIB lift-out from the indentation centre and TEM analysis

In order to observe the microstructure inside each indent, transmission electron microscopy (TEM, JEOL 2000FX) was carried out on thin foil samples lifted out from the 1 kg indents made in the alumina and 10% ZTA.

To prepare the lift-out samples, a focused ion beam system (Nova Nanolab 600, FEI) was used. Initially, a platinum protective layer was deposited on the diagonal of the indent, with an area of 20 μm × 1.5 μm and a thickness of ∼1.5 μm. Then, a 20 nA ion beam was used to mill two trenches measuring ∼25 μm × 15 μm in area and ∼10 μm in depth on each side of the platinum layer. A U-shaped cut was performed on the slice shaped material with one side not fully cut through, in order to prevent the sample from falling off. A sharp tungsten probe was welded to the edge of the slice using platinum deposition and then the bridge connecting the slice to the rest of the sample was cut and the sample was lifted out. The sample was attached onto a TEM copper grid using a platinum weld and then cleaned and thinned using a reduced ion beam current of 0.5 or 1 nA, to prevent sample damage. The final TEM sample measured ∼20 μm in width, 3–5 μm in length and ∼100 nm in thickness.

3. Results and discussion

The densities, grain sizes, mechanical properties and zirconia phase conditions of the samples to be studied are listed in Table 3.

3.1. Depth scanning and laser penetration

The depth scanning results of the Cr^{3+} fluorescence are shown in Fig. 3, which plots the R1 peak intensity, normalised

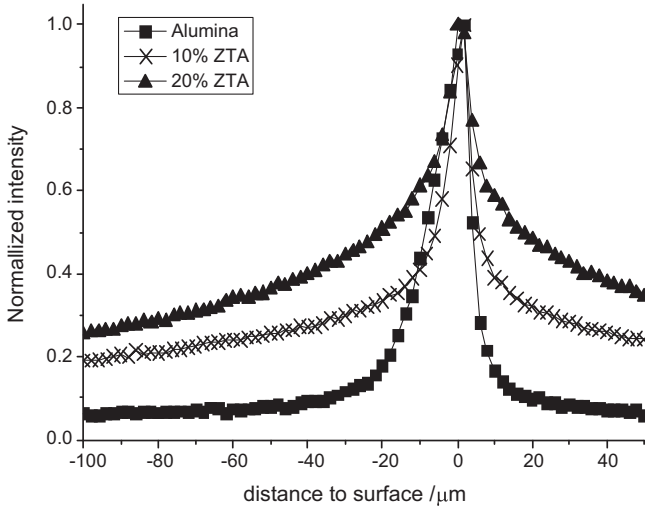

Fig. 3. Depth scanning on the polished surfaces of alumina, 10% ZTA and 20% ZTA; the intensity corresponds to the normalised intensity of the R1 fluorescence peak.

Table 3
Microstructural and mechanical properties of samples.

Sample code	Density (% theor.)	Mean grain size		Hardness (GPa)	Toughness (MPa $m^{1/2}$)	Percentage of t-ZrO_2 (%)
		Al_2O_3 (μm)	YSZ (nm)			
Alumina	99.0 ± 0.2	1.2	–	21.0 ± 0.4	3.0 ± 0.4	–
10% ZTA	99.0 ± 0.2	0.9 ± 0.1	170 ± 60	19.9 ± 0.3	5.2 ± 0.3	100
20% ZTA	99.3 ± 0.3	1.1 ± 0.1	280 ± 60	19.3 ± 0.3	5.3 ± 0.2	100

using the maximum intensity, covering stage displacements from −100 μm (i.e. focus is below the surface) to +50 μm. For all the three materials, alumina, 10% ZTA and 20% ZTA, the results show a sharp peak with the highest intensities near the surface, as expected. For the alumina, very little signal was collected once the focusing position was greater than 40 μm from the surface, whilst for the ZTAs, much broader shoulders were observed. This suggests a much larger sampling volume in the ZTAs. The results indicate that the addition of fine grain sized zirconia inclusions induced a very strong laser scattering effect, which increased with increasing zirconia content. The elastic scattering of light could have been caused by the larger number of particles and interfaces, resulting in a degradation of the confocal optics and therefore the illumination of a larger volume of the matrix and the scattering of more luminescent radiation towards the confocal aperture. Similar observations have been made in alumina/silicon carbide nanocomposites[12] but the effect is much stronger in the present alumina/zirconia ZTAs. This may be because zirconia absorbs much less light than SiC.

3.2. Cr^{3+} fluorescence analysis on the indentation centre – origin of the sharp peaks and broad peaks

The Cr^{3+} fluorescence spectra from the indent centres of the three materials are shown in Fig. 4. All the spectra were 4-peak fitted to separate the two doublets; examples of the curve fitting are shown in Fig. 5, which shows one doublet with broad R1 and R2 peaks and the other doublet with sharp R1 and R2 peaks in each example. The broad peaks, which displayed very significant negative peak shift and peak broadening, are believed to originate from within the plastic zone as the materials experienced extensive plastic deformation caused by the high compressive load during indentation. On the other hand, very limited peak shift and peak broadening were observed for the sharp peaks

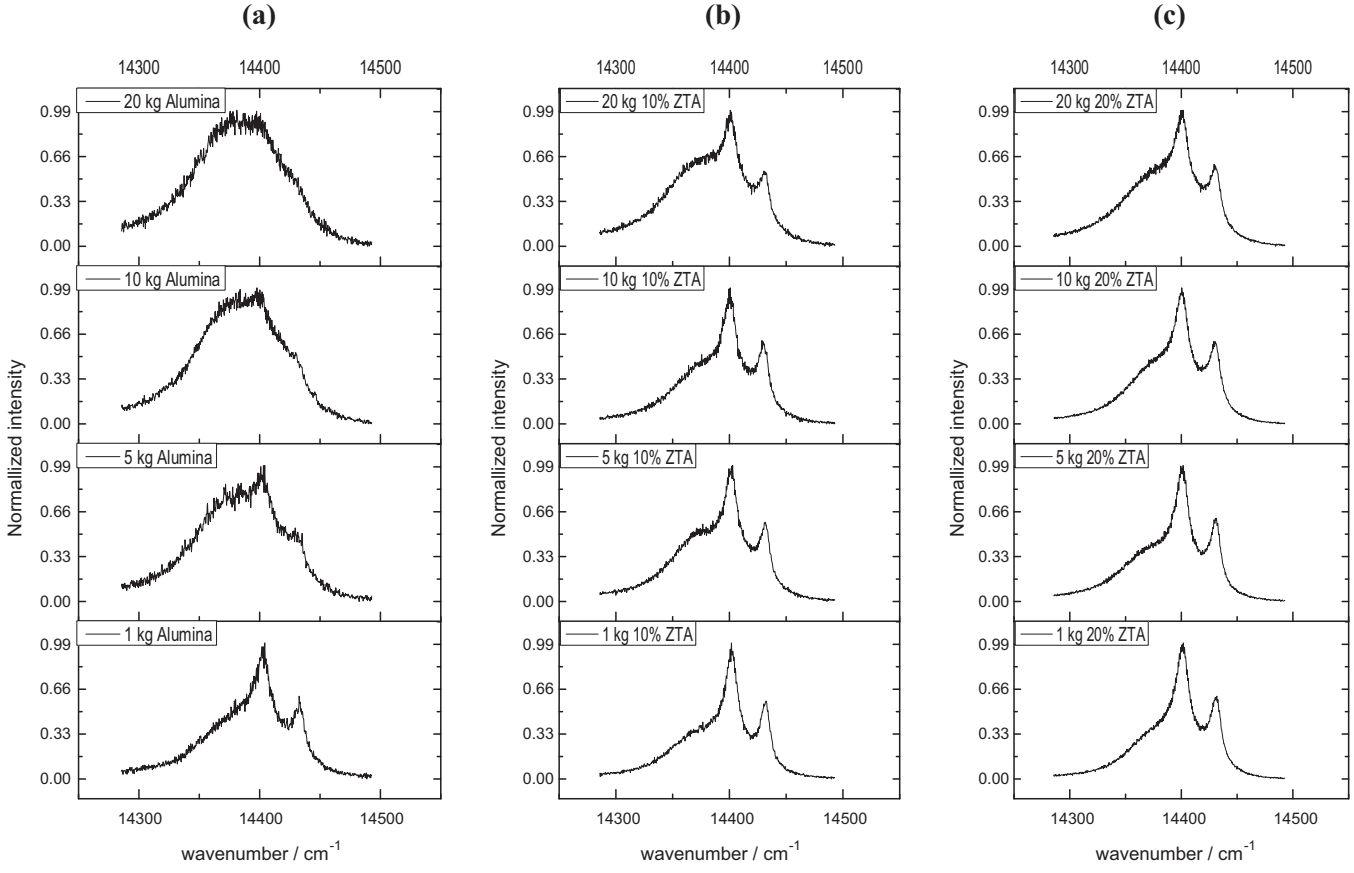

Fig. 4. Cr^{3+} fluorescence spectra collected from the indent centre for (a) alumina, (b) 10% ZTA and (c) 20% ZTA with indentation loads of 1, 5, 10 and 20 kg.

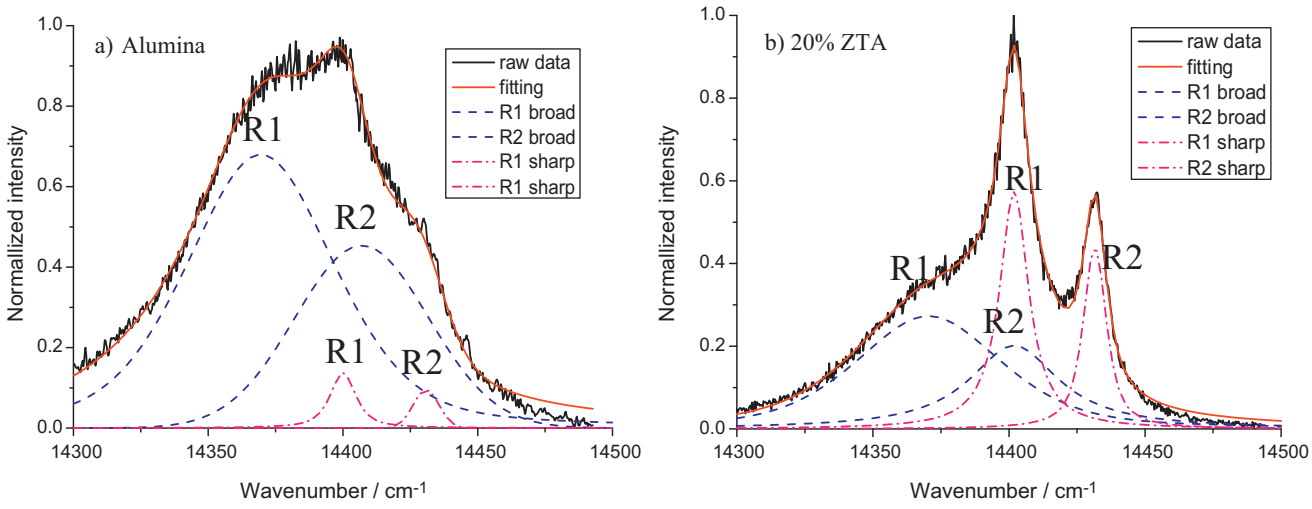

Fig. 5. Comparison of the 4-peak fitting results for the Cr^{3+} fluorescence spectra from the indent centres of (a) alumina and (b) 20% ZTA, both with the 10 kg indentation load.

from each sample, which suggests that these peaks may have originated from outside the plastic zone.

Measurements of broad peak percentage, peak shift and peak width were made on the broad peaks from the alumina, as a baseline material, and are listed in Table 4. The broad peak percentage was measured by calculating the area ratio of the broad R1 peak compared to the sum of the broad and sharp R1 peaks. When a 1 kg indentation was used, about 79% of the signal was collected from the plastic zone; the data also showed a ~32 cm^{-1} shift of the broad peak and broadening of ~56 cm^{-1}. This result is very consistent with that of Guo and Todd,[13] also with a 1 kg indentation, confirming the validity of the 4-peak fitting and similar resolution of the Raman equipment used in Guo's and the present studies. With increasing indentation load, the plastic zone size increased significantly from 15 to 100 μm. The percentages of broad peak in alumina were increased from 79% (1 kg) to 99% (20 kg); there was a sharp increase between 1 and 5 kg, which indicated that the plastic zone was large enough by the latter load to result in nearly all the collected signal originating from inside it. The comparison further demonstrated that the origin of the two doublets in the indentation area, i.e. the broad peaks, represented the signal from the plastic zone, whereas the sharp peaks were generated from the materials outside the plastic zone. In addition, with increasing indentation load, the peak shift and peak broadening were observed to increase slightly in the broad peaks, i.e. from 32 (1 kg) to 39 cm^{-1} (20 kg) for the shift and from 56 (1 kg) to 70 cm^{-1} (20 kg) for the broadening. This variation was limited in comparison to the extent of the increase in the indentation load and the size of the plastic zone, as expected, since the mean pressure is believed to remain approximately constant in the yield zone. During the indentation process, the plastic zone size increased as the load increased, continuously forming freshly yielded zones outside the previously formed plastic zone, without affecting the stress level beneath the indenter significantly.[19] The result also confirmed that the fitted broad peaks are physically meaningful and that the fitting work was applicable to the full range of indentation loads used in this study.

The same broad peak analysis was also performed on the ZTA samples. Compared to the case for alumina, the broad peak percentages were significantly reduced for the ZTA indentations for all the indentation loads. The values as a function of plastic zone size are shown in Fig. 6, confirming that the strong, sharp peak doublets in the ZTA originated from the material outside the plastic zone due to the much greater laser scattering with the ZTA samples.

3.3. *Effect of zirconia phase transformation on the residual stress distribution around indents*

After confirming the origins of the sharp and broad peaks in alumina and ZTA, the residual stresses at the indent centres formed under different loads were studied based on the peak shift of the broad R1 fluorescence peaks, as shown in Fig. 7. An increase in peak shift with increasing indentation load may be observed for all three materials, however, no significant difference can be observed in terms of their peak shift between alumina and ZTAs, which suggests that either the zirconia

Table 4
Quantitative analysis of the size of the plastic zone, broad peak percentage, peak shift and peak broadening condition on the indentation centre for a range of indentation loads for alumina.

Indentation load (kg)	Size of plastic zone (μm)	Measured broad peak (%)	Peak shift (cm^{-1})	Peak width change (cm^{-1})
1	15	78.8 ± 3.2	32.4	56.4
5	35	94.8 ± 5.0	32.8	56.9
10	60	96.3 ± 3.7	37.7	57.0
20	100	98.8 ± 2.5	39.3	70.4

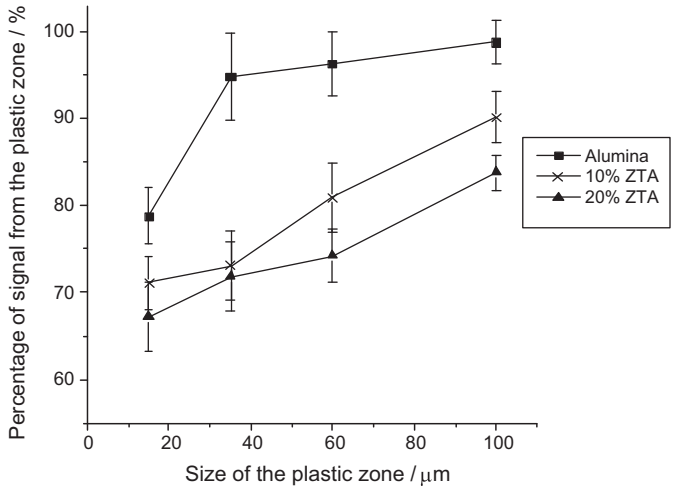

Fig. 6. Effect of indentation load on the broad peak percentage for the three different materials as a function of plastic zone size.

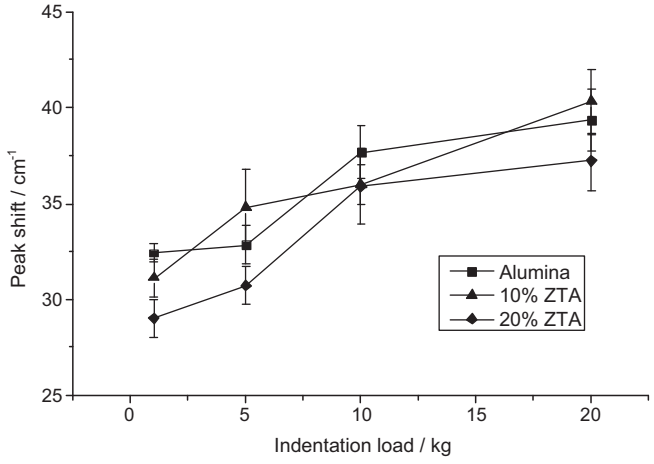

Fig. 7. R1 broad peak shift at the indent centres for the alumina, 10% ZTA and 20% ZTA specimens, with increasing indentation loads.

phase transformation did not happen at the indent centre or, if it did, it had a very limited effect on the residual stress change in the alumina grains. Determining which explanation was valid was achieved via Raman analysis of the zirconia phases inside and around the indents.

Fig. 8(a) shows an example of the line map obtained for the transformed monoclinic zirconia concentration from outside a 10 kg indent in 20% ZTA to its centre. The Raman spectra from three locations, viz. the indent centre, on the inclined surface inside the indent and at the surface outside the edge of the indent, are shown in Fig. 8(b). It may be seen that significant monoclinic peaks were observed around the indent, whilst their intensity reduced when focusing on the inclined surface of the indent and virtually no monoclinic peak was observed in the indent centre itself. It should be noted, however, that the intensity of the Raman signal reduced significantly when close to the indent centre, this will have affected the accuracy of the quantitative measurement. The reduction in intensity will have been caused by several factors, including the surface formed by the compression of the indenter being both concave and very rough compared to a polished surface, resulting in the refraction of the incident radiation, and being plastically deformed, disrupting the phonons responsible for the Raman effect. In addition, the relatively low zirconia contents (10–20%) meant that the intrinsic intensity of the Raman signal was very low.

A further factor that is important to note in interpreting these zirconia phase content results is that, like the Cr^{3+} fluorescence results, they reflect the phase content in the total sampling volume, some of which lies outside the immediate region on which the laser is focused, particularly in the ZTAs. Because of the greater breadth of the Raman peaks compared with the Cr^{3+} fluorescence peaks, however, the signal from the plastic zone cannot be extracted by multiple peak fitting. The phase contents measured should therefore be regarded as semi-quantitative.

Nevertheless, the trend of a reduction in the degree of zirconia phase transformation towards the indentation centre is very clear; a similar result was obtained by Paul et al.[20] for nano zirconia. The cause is believed to originate in the increasingly high compressive stresses towards the indent centre, which

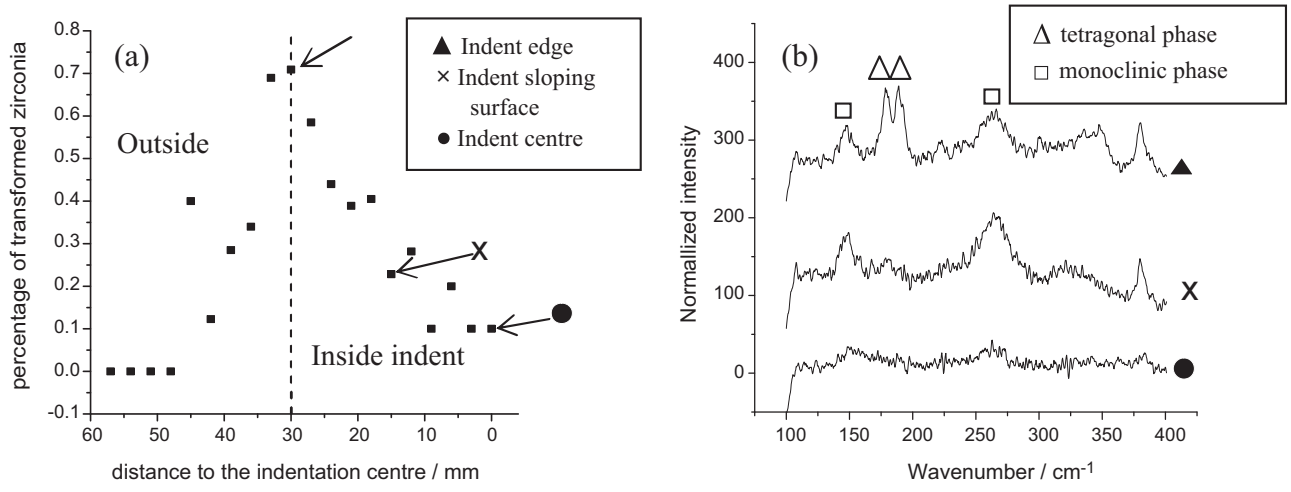

Fig. 8. (a) Raman line map obtained around a 10 kg indentation in 20% ZTA; (b) Raman spectra obtained at three locations on the same indent shown in (a).

Table 5
m-ZrO_2 contents on the indent of 10 and 20% ZTA with 5, 10 and 20 kg indent loads.

Material		10% ZTA			20% ZTA		
Indent load (kg)		5	10	20	5	10	20
m-ZrO_2 content/%	Indent edge	62	65	65	65	70	69
	Indent centre	10	12	9	11	11	14

will have suppressed the volume expansion that occurs during the phase transformation. However, the high monoclinic content near the edge of the indentation, where there are tensile stress components,[20] demonstrates unequivocally that the tetragonal to monoclinic transformation did take place in the region where permanent deformation was occurring as the indentation load increased. We tentatively suggest, therefore, that some of the monoclinic zirconia formed around the indenter during loading may also have transformed back to tetragonal zirconia as the indentation expanded and enveloped this initially transformed material in the highly compressive region beneath the indenter. Previous results on 3Y-TZP with conventional grain size[21] do not show this effect. One reason for this may be that the significantly higher stiffness of ZTA compared with 3Y-TZP is expected to lead to correspondingly higher compressive stresses in the plastic zone, which would favour reverse transformation. It may also reflect differences between the transformability of zirconia grains with grain sizes close to nano range and conventional materials and clearly merits further investigation.

The same experiments were carried out on the 10% ZTA and the indents with different loads. The same trend of reduction in the degree of zirconia phase transformation towards the indentation centre was observed. The results are listed in Table 5, in which only the content of transformed monoclinic zirconia phase on the edge of the indent and in the indent centre are displayed. It should be noted that an error of about ±5% was observed, due to the factors mentioned before which affected the accuracy of the quantitative measurements; within experimental error, no significant difference was observed with variation of either zirconia content or indentation load.

A line scan of the R1 peak shift with distance to the indent centre was made and the results are shown in Fig. 9. For all samples, the compressive residual stress increased significantly from the unloaded surface to the indent centre owing to the constraint on the expanded indentation region from the unyielded material surrounding it. The peak shift inside the indent, in the range of 30–10 μm from the indent centre, displayed consistently lower values for the ZTA samples compared to the alumina (Fig. 9). The mean difference was ~4 cm^{-1}, corresponding to a hydrostatic stress of ~500 MPa. Although there was virtually no zirconia monoclinic phase at the centre of the indent, the amount of transformation increased significantly on the inclined indent surface, particularly from 10 to 30 μm away from the centre (Fig. 8(a)). Therefore, it is very likely that the observed lower residual stresses in the ZTAs compared to the alumina originated from the zirconia phase transformation.

Gregori et al. [22] found that there was a linear relationship between the degree of zirconia phase transformation and the

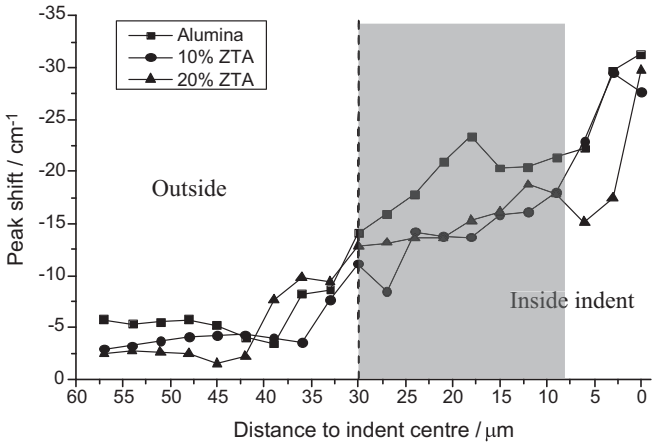

Fig. 9. R1 broad peak shift along a line from the sample surface to the indentation centre for the alumina, 10% ZTA and 20% ZTA specimens using a 10 kg load to create the indents. The dashed line separates the mapping positions inside and outside the indent, the grey area indicates the positions showing different peak shift between the alumina and ZTA samples.

residual tensile stress produced in the alumina matrix of ZTA. The explanation is that during the zirconia phase transformation process, the volume expansion of transformed zirconia grains is resisted by the surrounding alumina matrix putting the zirconia into compression and the alumina into tension.[23] Therefore, for ZTA materials after indentation testing, some alumina grains around the phase transformed zirconia received a fraction of the tensile stress, which cancelled part of the compressive stress induced by the indentation, resulting in the lower net residual stresses at the locations with zirconia phase transformation. According to the modelling results of Gregori et al.,[22] the maximum tensile stress provided by 100% zirconia phase transformation was about 600 MPa for ~20 vol% zirconia. This value is of a similar level to the measured difference in the residual stresses on the indentation surfaces of the alumina and ZTA samples. It is also interesting that there was little difference in matrix residual stress between the 10% and 20% ZTA. This suggests a smaller proportion of zirconia transformed to the monoclinic phase in the 20% ZTA but it is not possible to determine the veracity of this proposal because of the semi-quantitative nature of the phase content results noted above. The similar stress levels outside the indentation for all three ceramics can be understood in terms of their similar hardness values. This implies that the extra volume of the indentation that needs to be accommodated by elastic strains in the material around it is approximately the same. A further implication is that the mean residual stress within the plastic zone when the stress in the zirconia phase is accounted for in addition to the alumina matrix is also similar in all three materials.

3.4. Effect of zirconia phase transformation on the dislocation density distribution in the alumina around indents

The dislocation densities at the centre of the indents formed under different loads were compared using the peak width changes in the broad R1 fluorescence peaks, as shown in

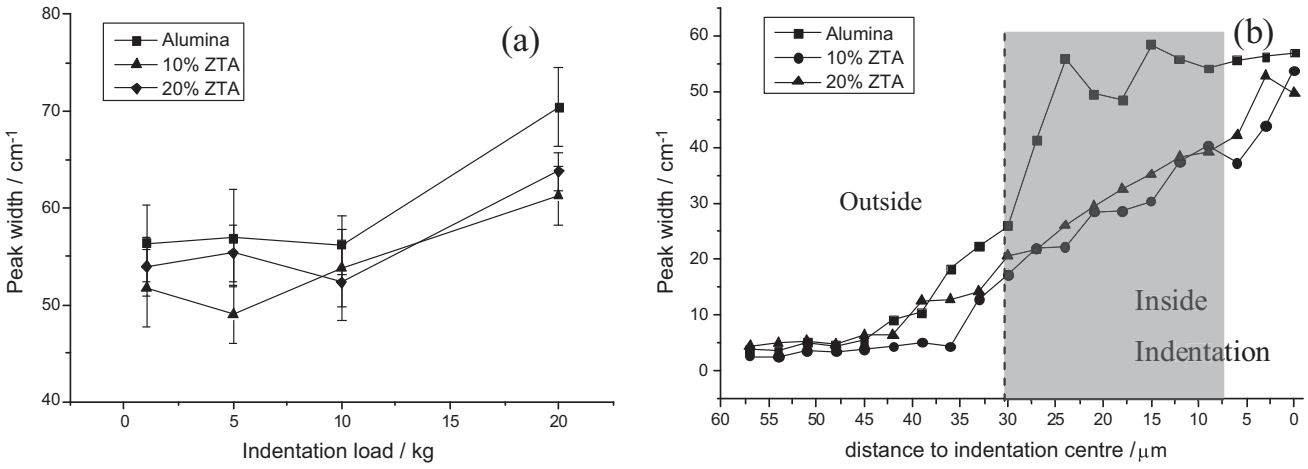

Fig. 10. R1 broad peak width change (a) at the indent centre and (b) along a line from the sample surface to the indentation centre of the alumina, 10% ZTA and 20% ZTA specimens using a 10 kg load to create the indents. The dashed line separates the mapping positions inside and outside the indent, the grey area indicates the positions showing different peak width change between the alumina and ZTA samples.

Fig. 10(a). In each case there was a clear increase in the peak broadening between the 10 and 20 kg indents, though it was less in the ZTA samples than the alumina. Assuming that dislocation formation was the dominant source of broadening, this indicates that the alumina dislocation densities at the indent centres of the ZTA materials were lower than in the pure alumina.

Following the same mapping points illustrated in Fig. 9, the peak width change from the unloaded surface to the indent centres for the 10 kg indentations are shown in Fig. 10(b). The alumina sample showed a sharp increase in the values around the edge of the indent and the change of peak width, from about 10 to 55 cm^{-1}, remained fairly constant within the indent. For the ZTAs, however, the peak width increased reasonably smoothly along most of the mapping route, until reaching a similar value to that of the alumina at the indent centre. This more gradual peak broadening associated with the ZTAs could also have originated from the zirconia phase transformation inside the indentations. It can be observed that the peak width difference between the ZTAs and alumina was gradually reduced nearer to the indent centre, which is again consistent with the trend of a reduced zirconia transformation, i.e. the fraction of monoclinic phase, from the edge of the indentation to its centre, as discussed in Section 3.3. The volume change during transformation could directly contribute to the deformation at the edge of the plastic

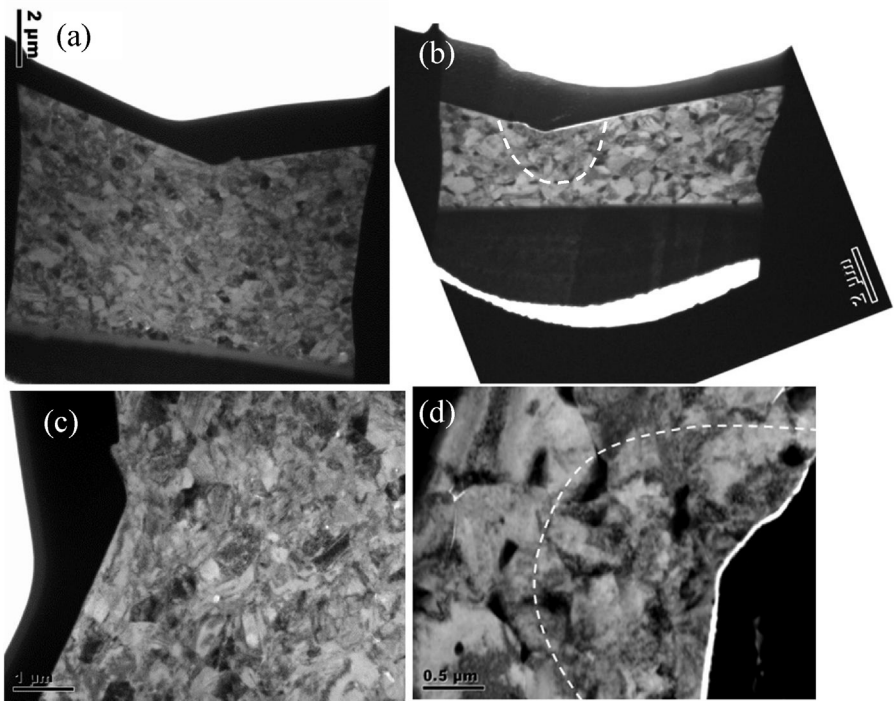

Fig. 11. TEM images of the FIB lift-out sample taken from a 1 kg indentation of (a) alumina and (b) 10% ZTA, (c) and (d) are higher magnification images of (a) and (b), respectively, at the indent centre.

zone during loading but could be magnified considerable when the large shear deformation (~0.16) also occurring is taken into account. In isotropic conditions, the net shear is effectively removed by twinning[24] but in the presence of a deviatoric stress, such as exists at the edge of the indentation,[19] the twinning will occur in order to minimise the mechanical energy of the system, producing potentially large net shear strains that can also contribute to the deformation process, leaving less requirement for dislocation and twinning mediated plastic deformation in the alumina matrix. Even if some reverse transformation does occur as indentation progresses, as suggested in Section 3.3, a residual ferroelastic switching may remain, preserving the shape of the indentation and again reducing the plastic strain contributed by the alumina matrix.

3.5. TEM analysis

As indicated earlier, in order to observe the microstructure inside the plastic zone, FIB lift-out was performed on the 1 kg indents of a 10% ZTA and an alumina sample. The samples were then characterised using TEM. The results are shown in Fig. 11. It should be noted that the sizes of the 1 kg indents on the ZTA and alumina samples were around 20 μm, which is comparable to the final electron transparent part of the TEM lamellae. Therefore, the TEM observation from these lamellae should be representative to the microstructure of the plastic zones in ZTA and alumina. For both samples, it was observed that there were very many dislocations inside the plastic zone, as expected. In the alumina sample, dislocation entanglements were observed across the whole lift-out sample area and the grain boundaries were not easily observed because of the high dislocation density (Fig. 11(a) and (c)). The situation was different for the 10% ZTA sample, however, where only the exact indent centre had a high dislocation density (as highlighted in Fig. 11(b) and (d)) and across the rest of the lift-out sample the grain boundaries could be observed clearly (Fig. 11(b) and (d)). This observation is consistent with the peak broadening mapping shown in Fig. 10(b).

4. Conclusions

The residual stresses around 1–20 kg indentations in alumina and 10% and 20% ZTA have been measured using Cr^{3+} fluorescence microscopy. According to depth scanning of the Cr^{3+} fluorescence peak intensity, a significant laser scattering effect in the ZTA samples was observed. The broad peaks were confirmed to be generated inside the plastic zone, due to the consistency of the measured percentage of R1 broad peak and the expected percentage of signal from inside the plastic zone with different indentation loads.

The peak shift analysis on the three materials showed no significant difference in the residual stresses in the indent centres between alumina and ZTA samples. This is believed to be because, in the ZTA samples, the zirconia phase transformation at the indent centre was suppressed by the high compressive stress. The degree of zirconia transformation increased, however, towards the edge of indent and the ZTA samples showed ~500 MPa reduction in the net compressive residual stress in the alumina matrix compared to the pure alumina sample. This was probably caused by the generation of tensile residual microstresses in the alumina grains due to the zirconia phase transformation. The similarity in stress around the indentations suggested the mean residual stress in the indentation plastic zone was the same for all three materials.

In addition, it was found that the ZTA materials displayed lower dislocation densities on the indentation surfaces away from the centre, where the zirconia phase transformation occurred. This effect was considered to be caused by the contribution of the zirconia transformation to the total deformation. The TEM study has shown that the plasitic zone microstructure of pure alumina and ZTA are different, which also confirms the observation from Cr^{3+} fluorescence study.

Acknowledgements

This research is part of the Understanding and Improving Ceramic Armour (UNICAM) project jointly funded by EPSRC and the Ministry of Defence, UK. The authors thank Prof. Peter Brown (DSTL), Dr. Chris Spacie (Morgan Electrical Carbon) and Dr. Chris Hampson (Morgan Technical Ceramics) for many valuable suggestions during the research.

References

1. Wang J, Stevens R. Review zirconia-toughened alumina (ZTA) ceramics. *J Mater Sci* 1989;**24**:3421–4344.
2. Casellas D, Nagl M, Llanes L, Anglada M. Fracture toughness of alumina and ZTA ceramics: microstructural coarsening effects. *J Mater Process Technol* 2003;**143–144**:148–52.
3. Magnani G, Brillante A. Effect of the composition and sintering process on mechanical properties and residual stresses in zirconia–alumina composites. *J Eur Ceram Soc* 2005;**25**:3383–92.
4. Bartolomé JF, De Aza AH, Martín A, Pastor JY, Llorca J, Torrecillas R, et al. Alumina/zirconia micro/nanocomposites: a new material for biomedical applications with superior sliding wear resistance. *J Am Ceram Soc* 2007;**90**:3177–84.
5. Zhang XF, Li YC. On the comparison of the ballistic performance of 10% zirconia toughened alumina and 95% alumina ceramic target. *Des Nanomater Nanostruct* 2010;**31**:1945–52.
6. Katagiri G, Ishida H, Ishitani A. Direct determination by a Raman microprobe of the transformation zone Size in Y_2O_3 containing tetragonal ZrO_2 polycrystals. *Adv Ceram* 1988;**24**:537–44.
7. Grabner L. Spectroscopic technique for the measurement of residual stress in sintered Al_2O_3. *J Appl Phys* 1978;**49**:580–3.
8. Ma Q, Clarke DR. Stress measurement in single-crystal and polycrystalline ceramics using their optical fluorescence. *J Am Ceram Soc* 1992;**76**:1433–40.
9. He J, Clarke DR. Determination of the piezospectroscopic coefficients for chromium-doped sapphire. *J Am Ceram Soc* 1995;**78**:1347–53.
10. Ma Q, Pompe W, French J, Clarke DR. Residual stresses in Al_2O_3–ZrO_2 composites: a test of stochastic stress models. *Acta Metal Mater* 1994;**42**:1673–81.
11. Wu HZ, Roberts SG, Derby B. Residual stress distributions around indentations and scratches in polycrystalline Al_2O_3 and Al_2O_3/SiC nanocomposites measured using fluorescence probes. *Acta Mater* 2008;**56**:140–9.
12. Guo S, Todd RI. Confocal fluorescence microscopy in alumina-based ceramics: where does the signal come from. *J Eur Ceram Soc* 2010;**30**:641–8.
13. Guo S, Todd RI. Quantitative optical fluorescence microprobe measurements of stresses around indentations in Al_2O_3 and Al_2O_3/SiC

nanocomposites: the influence of depth resolution and specimen translucency. *Acta Mater* 2011;**59**:2637–47.
14. Santacruz I, Anapoorani K, Binner J. Preparation of high solids content nanozirconia suspensions. *J Am Ceram Soc* 2008;**91**:398–405.
15. Binner JGP, Santacruz MI, Annapoorani K. Method for concentrating nanosuspensions. International patent application Publ. No. WO 2006/136780 A2, Publ. Date 28/12/2006.
16. Binner JGP, Vaidhyanathan B. Processing of bulk nanostructured ceramics. *J Eur Ceram Soc* 2008;**28**:1329–39.
17. Clarke DR, Adar F. Measurement of the crystallographically transformed zone produced by fracture in ceramics containing tetragonal zirconia. *J Am Ceram Soc* 1982;**65**:284–8.
18. Guo S, Todd RI. Cr^{3+} microspectroscopy measurements and modelling of local variations in surface grinding stresses in polycrystalline alumina. *J Eur Ceram Soc* 2010;**30**:2533–45.
19. Yoffe EH. Elastic stress fiels caused by indenting brittle materials. *Philos Mag A* 1982;**46**:617–28.
20. Paul A, Vaidhyanathan B, Binner J. Micro-Raman spectroscopy of indentation induced phase transformation in nanozirconia ceramics. *Adv Appl Ceram* 2011;**110**:114–9.
21. Muñoz-Tabares JA, Jiménez-Piqué E, Reyes-Gasga J, Anglada M. Microstructural changes in 3Y-TZP induced by scratching and indentation. *J Eur Ceram Soc* 2012;**32**:3919–27.
22. Gregori G, Burger W, Sergo V. Piezo-spectroscopic analysis of the residual stresses in zirconia-toughened alumina ceramics: the influence of the tetragonal-to-monoclinic transformation. *Mater Sci Eng A* 1999;**271**:401–6.
23. Sergo V, Clarke D, Pompe W. Deformation bands in ceria stabilized tetragonal zirconia/alumina: I, measurement of internal stresses. *J Am Ceram Soc* 1995;**78**:633–40.
24. Kelly PM, Ball CJ. Crystallography of stress-induced martensitic transformations in partially stabilized zirconia. *J Am Ceram Soc* 1986;**69**:259–64.